

Original Article

Computed tomography and magnetic resonance imaging features of solitary langerhans cell histiocytosis in calvaria

Hexiang Wang¹, Pei Nie¹, Cheng Dong¹, Jie Li¹, Jihua Liu¹, Yonghua Huang², Wenjian Xu¹

¹Department of Radiology, The Affiliated Hospital of Qingdao University, Qingdao, Shandong, China; ²Department of Radiology, The Puyang City Oilfield General Hospital, Puyang, Henan, China

Received September 16, 2016; Accepted December 19, 2016; Epub February 15, 2017; Published February 28, 2017

Abstract: Purpose: To assess the computed tomography (CT) and magnetic resonance imaging (MRI) features of Langerhans cell histiocytosis (LCH) in calvaria. Methods: The CT and MRI manifestations of 12 pathologically proven cases of solitary LCH involving the cranial bone were retrospectively analyzed. Assessed image features included: Location, size (soft-tissue mass and bone destruction), shape (soft-tissue mass and bone destruction), margins, attenuation and changes in adjacent bone on CT, and signal intensity and enhancement pattern on MRI. Results: The lesions were solitary, lytic, punched out, round to oval or geographic (size larger than 3 cm); With the appearance of bone destruction with a gourd-shape (n=12); And a soft-tissue mass extending from the subcutaneous to the intracranial space. On CT, a beveled edge was seen in all cases and button sequestration in two cases, but sclerotic rim was not evident. The hypoattenuated soft-tissue mass was mostly with patches of slight hypoattenuation spot (6/9 cases). On MRI, all cases showed long or iso-T1 and heterogeneous high T2 signal intensity relative to the brain. Diffusion-weighted images displayed mild hyperintensity (5/7 cases) or a low hypointensity (n=2). Postcontrast MR images demonstrated heterogeneous marked enhancement (n=7). A tail of dural and galea enhancement was seen in all cases. The adjacent bone marrow (4/10 cases) exhibited low intensity on T1-weighted images without gadolinium enhancement. Conclusion: Although the diagnosis of a calvarial LCH mainly depends on pathology, the imaging findings have value as well. CT and MRI have their own advantages in the diagnosis of LCH. Combined application of CT and MR examinations is recommended for patients with suspected LCH.

Keywords: Langerhans cell histiocytosis, skull, tomography, X-ray computed, magnetic resonance imaging

Introduction

Langerhans cell histiocytosis (LCH) is one of the histiocytoses originating from dendritic cells, in which there is abnormal accumulation of Langerhans cells in one or multiple organ systems. Because of the finding of cancer-associated gene mutations of the ERK pathway in this disease [1, 2], LCH has recently been classified as a myeloid neoplasm. The cancer cells can accumulate in virtually any organ, including bone, liver, lungs, spleen, and lymph nodes. LCH is a rare disease that predominantly affects the bone. So far, the calvaria are the most frequent site of involvement, usually affecting 45% of LCH patients [3]. However, in cranial bone, solitary LCH features have not been well specified. LCH may show similar imaging features with dermoid and epidermoid

cysts for single lesions, and with leukemia, lymphoma, multiple myeloma, and metastases for multiple lesions. Osteomyelitis must also be considered [4, 5]. At initial presentation of the disease, there have been few studies describing the imaging features of calvarial bone LCH [6-12]. The purpose of this retrospective study was to comprehensively assess the characteristic computed tomography (CT) and magnetic resonance imaging (MRI) findings regarding LCH in the cranial bone.

Materials and methods

Patients

This study was approved by our institutional ethics committee. Between July 2003 and January 2015, CT (9/12) and MRI (10/12) scans

Imaging features of LCH in calvaria

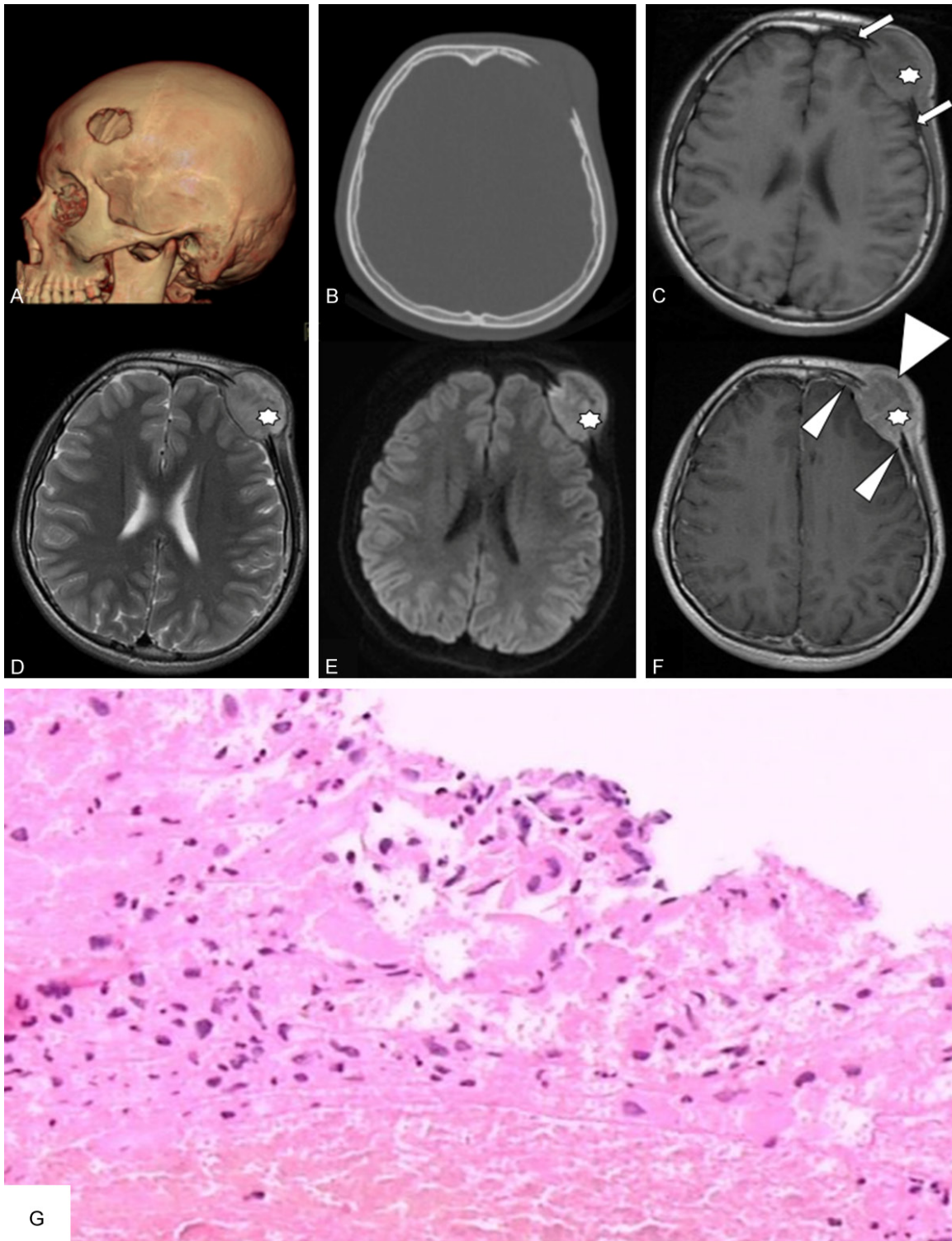


Figure 1. (A-G) A 15-year-old male patient with a known case of Langerhans cell histiocytosis. Non-enhanced computed tomography (CT) images of the head. (A) Volume-rendered image and (B) Axial view; Bone-window images show solitary, punched-out, oval, and lytic lesions in the left-side frontal bone. The bone destruction lesions demonstrate a beveled edge with no sclerotic rim. (C-F) Magnetic resonance images of the brain; Axial T1- and T2-weighted, diffusion-weighted images and contrast-enhanced images display a gourd-shaped soft-tissue mass (asterisk) extending from the subcutaneous to the intracranial space. The soft-tissue lesion shows heterogeneous long T1 and heterogeneous long T2 signal intensity relative to the brain. The diffusion-weighted image displays mild hyperintensity. Postcontrast magnetic resonance imaging scan shows heterogeneous marked enhancement with a tail of dural

Imaging features of LCH in calvaria

(small arrowheads) and galeal (large arrowhead) enhancement. The adjacent bone marrow shows low intensity on T1-weighted images (arrow) without gadolinium enhancement. Photomicrograph (G) shows that the lesion consists of diffusely infiltration of numerous Langerhans cells with scattered histiocyte-like cells, the hyperplasia of bone and Collagen fiber. (H&E, 100).

Table 1. The common or differences feature of calvarial LCH compared in CT and MRI

Image feature	Examination	CT	MRI
Patients number		9 (enhanced 0)	10 (enhanced 7)
Change of bone	Beveled edge	9	10
	Button sequestration	2	1
Change of adjacent bone marrow		0	4
Dural/galea enhancement		0	7

obtained from 12 patients (nine males and three females) with a median age of 14 (range, 1-42) years with pathologically proven LCH were retrospectively analyzed. The main clinical manifestations included soft-tissue swelling in the scalp (n=10), focal pain (n=7), fever (n=2), and exophthalmos (n=1). The duration of symptoms prior to diagnosis ranged from 2 months to 3 years (median, 1 year). All 12 patients had undergone surgery for their disease. Among the 12 patients, nine were referred for CT scanning and 10 for MRI (diffusion-weighted imaging [n=7]). Seven patients underwent postcontrast T1-weighted imaging.

CT scans were obtained using a standard CT protocol for the head. Nine patients underwent 5-mm-thick axial CT scanning using a soft-tissue algorithm, and all images were reformatted using a soft-tissue algorithm without the use of contrast media. Reformatted coronal, sagittal and volume-rendered images were also obtained (n=5). MRI examinations were performed using a 1.5 T MR scanner (n=4) (Signe Advantage Horizon: GE Medical Systems, Milwaukee, WI, USA) or a 3.0 T MRI scanner (n=6) (signal HDx: GE Medical Systems) with an 8-channel head coil. In these patients, precontrast T1-weighted spin-echo images and T2-weighted fast spin-echo images (n=10), diffusion-weighted imaging (b=0; 1000 s/mm²; n=7), were obtained, followed by contrast-enhanced T1-weighted spin-echo images with fat saturation after the intravenous injection of 0.1 mmol/kg of gadolinium dimeglumine in seven patients.

Imaging analysis

Two neuroradiologists who have worked for >10 years were blinded to the clinical and pathologi-

cal findings; They independently reviewed the location, size (soft-tissue mass and bone destruction), shape (soft-tissue mass and bone destruction), margins (well-defined or ill-defined), attenuation on precontrast CT, changes in the adjacent bone on bone-window CT, signal intensity on precontrast MRI and enhance-

ment pattern on contrast-enhanced MRI. The attenuation or signal intensity of the lesion was compared with that of the brain parenchyma. For location, the particular bone with lesion involvement was recorded (frontal bone, parietal bone or occipital bone). The size of each lesion was measured at its greatest single dimension.

Results

Patient symptoms were a soft-tissue mass in 83.3% (10/12), focal pain in 58.3% (7/12), fever in 16.7% (2/12), and exophthalmos in 8.3% (1/12). Five lesions were located in the parietal bone, three in the frontal bone, one in the frontal and orbit bone, and three in the occipital bone. Histopathological examination (**Figure 1G**) revealed that the skull lesion consisted of diffuse infiltration of Langerhans cells and histiocyte-like cells with a distinct cell margin, nuclear grooves, eosinophilic cytoplasm, and intranuclear inclusions. In addition, various inflammatory cells such as eosinophils, neutrophils, lymphocytes, and macrophages had also infiltrated. Furthermore, the histiocyte-like cells were immunohistochemically positive for S-100, CD1a, and CD68. The final histological diagnosis was LCH. The dura and galea showed no infiltration of Langerhans cells but mild infiltration of lymphocytes. The adjacent bone marrow (4/10) was infiltrated by Langerhans cells, and they were also positive for CD1a and CD68. The Ki-67 index ranged from 10% to 50%. During the follow-up period, which ranged from 6 months to 8 years, no patients experienced recurrence.

The CT and MRI features of the 12 patients with cranial LCH are summarized in **Table 1**. The lesions were solitary, lytic, and punched

Imaging features of LCH in calvaria

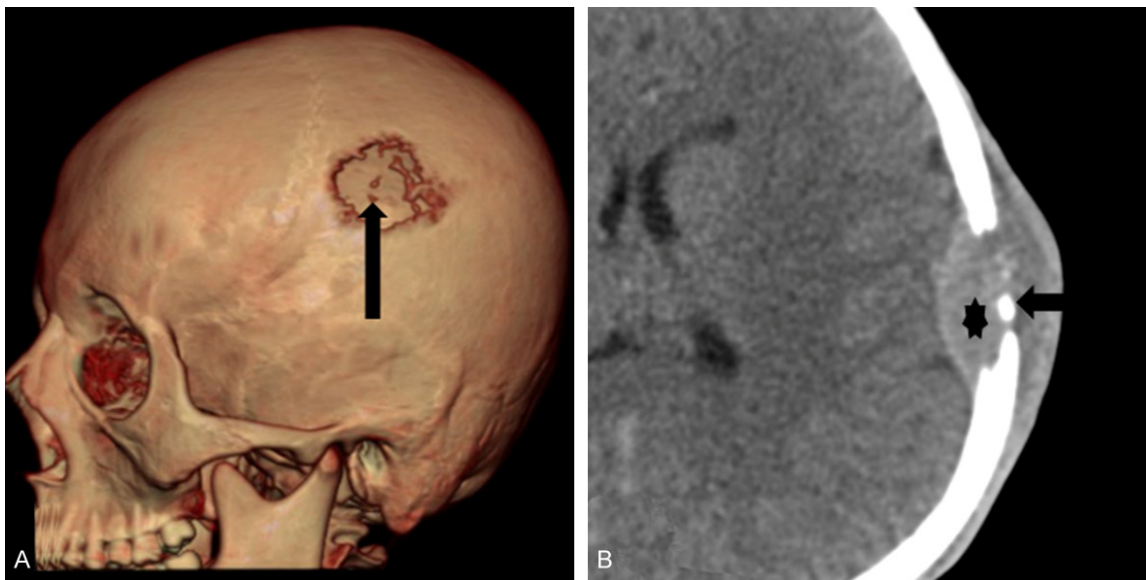


Figure 2. (A) and (B) A male patient aged 14 years with a known case of Langerhans cell histiocytosis. Non-enhanced computed tomography images of the head. (A) Volume-rendered image and (B) Axial view; Soft-tissue window images show solitary, punched-out, geographic, and lytic lesions in the left parietal bone. Bone destruction lesions showing a beveled edge with small residual bone fragments were seen in the soft-tissue mass representing button sequestration (arrow). The computed tomography image displays a hyperattenuated gourd-shaped soft-tissue mass extending from the subcutaneous to the intracranial space (asterisk).

out. The diameter of the soft-tissue mass ranged from 13.4 to 38.1 mm with a mean of 23.2 mm. All of the lesions had the appearance of a gourd-shaped soft-tissue mass extending from the subcutaneous to the intracranial space. The diameter of the bone destruction areas ranged from 1.2 to 2.9 cm; They were round to oval in shape (**Figure 1A**), but the other two with a size larger than 3 cm had a geographic (**Figure 2A**) appearance. Nine of the 10 lesions were examined using CT. On bone-window CT, the skull lesion appeared to have an unequal involvement of the inner and outer tables resulting in a beveled edge (**Figures 1B, 2B and 3A**), and was seen in all cases; Button sequestration (**Figure 2B**) was seen in two cases. A sclerotic rim was not observed in any of the lesions. The soft-tissue mass (6/9) was mostly hypoattenuated with patches of slight hypoattenuation.

Among the 12 patients, 10 were referred for MRI scanning. All cases showed long or iso-T1 (**Figures 1C and 3B**) and heterogeneous long T2 (**Figures 1D and 3C**) signal intensity relative to the brain. Diffusion-weighted imaging showed mild hyperintensity (5/7) (**Figure 1E**) or low hypointensity (n=2) (**Figure 3D**). Post-contrast MRI scanning revealed heterogeneous marked enhancement (n=7). A tail of

dural and galea enhancement was seen in all cases (**Figure 1F**). In four cases the soft-tissue mass adjacent to the bone marrow demonstrated low intensity on T1-weighted images without gadolinium enhancement (**Figure 1C**).

Discussion

LCH is a rare group of disorders with a wide range of clinical presentations that range from a solitary lesion to more severe multifocal or disseminated lesions [13, 14]. The solitary lesions were seen in approximately 70% of LCH cases [6]. LCH is a rare disease in the general population, with an estimated incidence of 1-2 adult cases per 1,000,000 annually, and 3-5 pediatric cases per 1,000,000 annually [15]. Most patients range in age from 1 to 15 years [1], and the disease occurs more commonly in males [16]. The findings of our study were basically similar to these findings. Patient age ranged from 1 to 42 years, with nine of 12 patients presenting at an age <15 years (median, 14 years). We could identify only three patients who were >18 years old who had this rare disease. In our study, the male to female ratio was 3:1, in agreement with previous studies [12, 17]. The clinical presentation of patients with LCH varies depending on the sites and extent of involvement. Skull lesions can be

Imaging features of LCH in calvaria

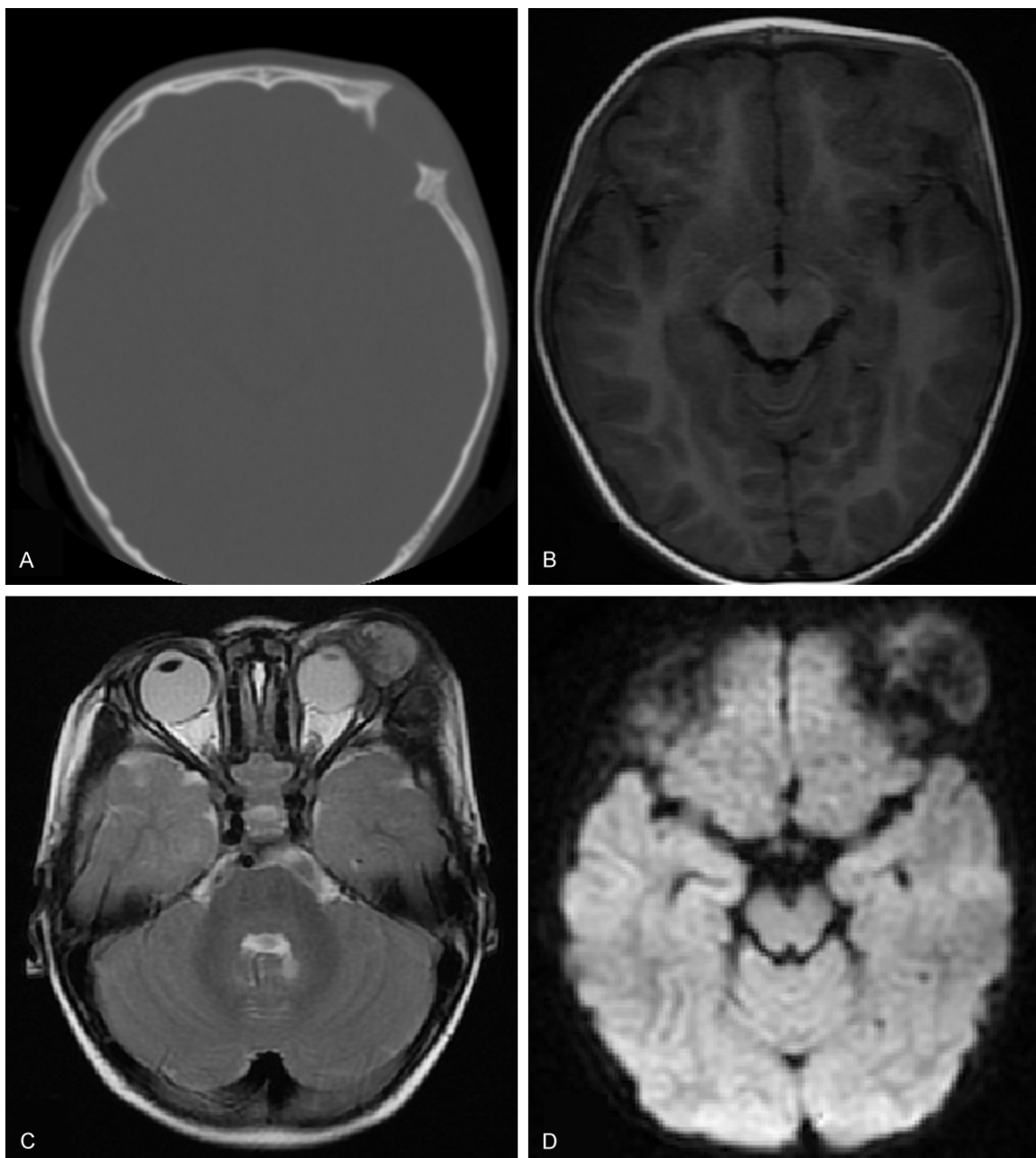


Figure 3. A-D. A female patient aged 42 years with a known case of Langerhans cell histiocytosis. Non-enhanced computed tomography images of the head. A. Axial view; Bone-window images show solitary, punched-out, and oval lytic lesions in the left-side frontal bone. The bone destruction lesions demonstrate a beveled edge with no sclerotic rim. B-D. Magnetic resonance imaging of the brain, axial T1- and T2-weighted, diffusion-weighted images display a gourd-shaped soft-tissue mass extending from the subcutaneous to the intracranial space; The lesion also involves the orbital cavity. The soft-tissue lesions show high T1 and heterogeneously high T2 signal intensity relative to the brain. The diffusion-weighted image displays limited hypointensity.

asymptomatic but may manifest with soft-tissue swelling in the scalp, focal pain, fever and exophthalmos.

In patients with calvarial LCH involvement, the parietal and frontal bones are the most com-

monly affected [4]. In the present study, the parietal (n=5) and frontal (n=4) bones were involved. The radiographic appearance of osseous LCH depended on the site and extent of involvement, and the phase of the disease. The calvarial LCH lesion has characteristic features

Imaging features of LCH in calvaria

on CT images. According to the literature and the present study, the typical imaging appearance of calvarial LCH on CT images is as follows: (I) Punched-out or identified centrally destructive lesions with non-sclerotic margins [12, 18]; (II) The skull lesion had an unequal involvement in the inner and outer tables, resulting in a characteristic beveled edge; (III) Bone destruction with a round to oval appearance or geographic (>3 cm) in shape [9, 12, 18]; (IV) A small bony fragment known as button sequestration seen near the skull defect; (V) A heterogeneous hyperattenuated soft-tissue mass; And (vi) soft tissue with marked CT contrast enhancement [12]. Remarkably, the presence of a beveled border was detected, which is a typical feature in the diagnosis of LCH [11, 12]. In addition, the presence of a button sequestrum which is less commonly seen, as reported by Vikas et al. [4], also provided clues for the diagnosis of LCH [11, 12].

The CT images of calvarial LCH also demonstrated a characteristic appearance with a gourd-shaped heterogeneous hyperattenuated soft-tissue mass extending from the subcutaneous to the intracranial space, an aspect that has not been emphasized in previous studies. LCH in flat bones and lytic lesions usually arises in the medullary space and extends to produce a periosteal reaction [9]; However, in our study none of the cases had a periosteal reaction. CT had the advantage of displaying the extent of lesions, and was better suited to demonstrating bone detail [19]; However, it was difficult to accurately display the extent of intracranial involvement, and reactive changes in the dura and galea. In addition, CT scans cannot reveal adjacent bone marrow invasion.

In current reports on calvarial LCH it has been clarified that MRI can detect isointense to hypointense regions on T1-weighted images and hyperintense regions on T2-weighted images (some cases show heterogeneity [18]); Variable contrast enhancement has been reported for reactive dural and/or galeal tissue enhancement [8, 12, 18, 20, 21]. In some reports involving the comparison of MRI and histological data, the finding of the meningioma 'dural tail sign' similar to skull LCH is one of the nontumoral enhancements seen on MRI; Gadolinium-enhanced dura mater and galeal tissue inflammatory cells have been reported to be present, but tumor cells were not seen [8]. The findings of the present study are in

accordance with the MRI signal characteristics previously mentioned.

The MRI signal characteristics lacked specificity for calvarial LCH identification. MRI revealed the extent of intracranial involvement and reactive changes in the dura and galea more clearly and precisely than CT [18, 19]. MRI also displayed a characteristic appearance, with the gourd-shaped soft-tissue mass extending from the subcutaneous to the intracranial space. Diffusion-weighted imaging displayed mild hyperintensity (5/7) or low hypointensity (n=2). All postcontrast MR images demonstrated a tail of dural enhancement and galeal enhancement. The adjacent bone marrow (4/10) shows low intensity on T1-weighted images without gadolinium enhancement, and proved to have Langerhans cell invasion at surgery; Pathognomonic Langerhans cells were seen in this portion as reported by Shinya et al. [8]. Bone marrow involvement is usually associated with poor prognosis [22, 23]. However, all our cases (n=4) had no recurrence in the follow-up period, and probably need additional observation time. Remarkably, the presence of these signs has not been emphasized in the past literature. Although no single finding is specific to the disease, the constellation of these findings seems to be suggestive of calvarial LCH and is helpful concerning the differential diagnosis.

Based on previous experience, the appearance of solitary lytic skull LCH on CT and MRI may cause the radiologist to misdiagnose the mass as dermoid cysts, epidermoid and hemangioma for single lesions [4, 5, 12]. Epidermoid and dermoid cysts are most commonly seen in midline locations, and are sometimes associated with a sinus tract; Because the content of the cyst varies (fat in dermoid cysts and fluid in epidermoid cysts); The CT attenuation and MRI signal intensity vary [24]. Intracranial epidermoid cysts [25, 26] have markedly high signal intensities on diffusion-weighted images, and may make a noteworthy contribution to differential diagnosis. Margins that are not sclerotic or beveled that can also occur in other benign skull lesions may be a noteworthy contribution to differential diagnosis, such as hemangiomas; However, they have been reported to have a characteristic honeycomb or sunburst pattern of bony spicules radiating from the center of a radiolucent round or oval defect [27]. Additionally, the signs of adjacent bone marrow

invasion can also exclude all of these benign lesions.

Conclusions

In conclusion, although the diagnosis of a calvarial LCH mainly depends on pathology, the imaging findings have value as well. MRI is the most valuable imaging technique for diagnosing calvarial LCH. The lesions seen in this study appeared as gourd-shaped soft-tissue mass extending from the subcutaneous to the intracranial space, with the lesions' adjacent dural and galea enhancement. The lesions showed isointense to hypointense signaling on T1-weighted images and hyperintense signaling on T2-weighted images and variable contrast enhancement on postcontrast MR images. Sometimes the adjacent bone marrow exhibited low intensity on T1-weighted images without gadolinium enhancement indicative Langerhans cell invasion. CT displayed hypoattenuated soft-tissue mass with a beveled edge and/or button sequestration. Such imaging findings are highly suggestive of a calvarial LCH.

CT and MRI have different advantages in the diagnosis of calvarial LCH. Preoperative CT images that display the characteristic appearance of the lesion can provide clues regarding the diagnosis of LCH. Preoperative T1-weighted images can detect Langerhans cell invasion in the skull bone marrow. Postcontrast MR images more precisely delineate the extracranial and intracranial soft-tissue components affected by the calvarial lesions, and can provide an accurate basis for the determination of the surgical scope. Therefore, combined application of CT and MR examinations is necessary for patients with suspected LCH.

Disclosure of conflict of interest

None.

Address correspondence to: Wenjian Xu, Department of Radiology, The Affiliated Hospital of Qingdao University, 16 Jiangsu Road, Qingdao, Shandong, China. Tel: +86 53282911585; E-mail: 178532-99558@163.com

References

[1] El Demellawy D, Young JL, de Nanassy J, Chernetsova E and Nasr A. Langerhans cell histiocytosis: a comprehensive review. *Pathology* 2015; 47: 294-301.

[2] Badalian-Very G, Vergilio JA, Degar BA, MacConaill LE, Brandner B, Calicchio ML, Kuo FC, Ligon AH, Stevenson KE, Kehoe SM, Garraway LA, Hahn WC, Meyerson M, Fleming MD and Rollins BJ. Recurrent BRAF mutations in Langerhans cell histiocytosis. *Blood* 2010; 116: 1919-1923.

[3] D'Ambrosio N, Soohoo S, Warshall C, Johnson A and Karimi S. Craniofacial and intracranial manifestations of langerhans cell histiocytosis: report of findings in 100 patients. *AJR Am J Roentgenol* 2008; 191: 589-597.

[4] Chaudhary V, Bano S, Aggarwal R, Narula MK, Anand R, Solanki RS and Singh P. Neuroimaging of Langerhans cell histiocytosis: a radiological review. *Jpn J Radiol* 2013; 31: 786-796.

[5] Khung S, Budzik JF, Amzallag-Bellenger E, Lambilliotte A, Soto Ares G, Cotten A and Boutry N. Skeletal involvement in Langerhans cell histiocytosis. *Insights Imaging* 2013; 4: 569-579.

[6] Zaveri J, La Q, Yarmish G and Neuman J. More than just Langerhans cell histiocytosis: a radiologic review of histiocytic disorders. *Radiographics* 2014; 34: 2008-2024.

[7] Stull MA, Kransdorf MJ and Devaney KO. Langerhans cell histiocytosis of bone. *Radiographics* 1992; 12: 801-823.

[8] Watanabe S, Yamamoto T, Satomi K, Matsuda M, Akutsu H, Ishikawa E and Matsumura A. Comparison of magnetic resonance imaging with invasive histological findings of Langerhans cell histiocytosis. *Brain Tumor Pathol* 2014; 31: 182-186.

[9] Herman TE and Siegel MJ. Langerhans cell histiocytosis: radiographic images in pediatrics. *Clin Pediatr (Phila)* 2009; 48: 228-231.

[10] Lee SK, Jung TY, Jung S, Han DK, Lee JK and Baek HJ. Solitary Langerhans cell histiocytosis of skull and spine in pediatric and adult patients. *Childs Nerv Syst* 2014; 30: 271-275.

[11] Chen HC, Shen WC, Chou DY and Chiang IP. Langerhans cell histiocytosis of the skull complicated with an epidural hematoma. *AJNR Am J Neuroradiol* 2002; 23: 493-495.

[12] Okamoto K, Ito J, Furusawa T, Sakai K and Tokiguchi S. Imaging of calvarial eosinophil granuloma. *Neuroradiology* 1999; 41: 723-728.

[13] Arkader A, Glotzbecker M, Hosalkar HS and Dormans JP. Primary musculoskeletal Langerhans cell histiocytosis in children: an analysis for a 3-decade period. *J Pediatr Orthop* 2009; 29: 201-207.

[14] Martinez-Lage JF, Poza M, Cartagena J, Vicente JP, Biec F and de las Heras M. Solitary eosinophilic granuloma of the pediatric skull and spine. The role of surgery. *Childs Nerv Syst* 1991; 7: 448-451.

[15] Baumgartner I, von Hochstetter A, Baumert B, Luetolf U and Follath F. Langerhans'-cell histio-

Imaging features of LCH in calvaria

- cytosis in adults. *Med Pediatr Oncol* 1997; 28: 9-14.
- [16] Nicholson HS, Egeler RM and Nesbit ME. The epidemiology of Langerhans cell histiocytosis. *Hematol Oncol Clin North Am* 1998; 12: 379-384.
- [17] Cochrane LA, Prince M and Clarke K. Langerhans' cell histiocytosis in the paediatric population: Presentation and treatment of head and neck manifestations. *J Otolaryngol* 2003; 32: 33-37.
- [18] De Schepper AM, Ramon F and Van Marck E. MR imaging of eosinophilic granuloma: Report of 11 cases. *Skeletal Radiol* 1993; 22: 163-166.
- [19] Azouz EM, Saigal G, Rodriguez MM and Podda A. Langerhans' cell histiocytosis: Pathology, imaging and treatment of skeletal involvement. *Pediatr Radiol* 2005; 35: 103-115.
- [20] Buchmann L, Emami A and Wei JL. Primary head and neck Langerhans cell histiocytosis in children. *Otolaryngol Head Neck Surg* 2006; 135: 312-317.
- [21] Mut M, Cataltepe O, Bakar B, Cila A and Akalan N. Eosinophilic granuloma of the skull associated with epidural haematoma: a case report and review of the literature. *Childs Nerv Syst* 2004; 20: 765-769.
- [22] Braier J, Chantada G, Rosso D, Bernaldez P, Amaral D, Latella A, Balancini B, Masautis A and Goldberg J. Langerhans cell histiocytosis: retrospective evaluation of 123 patients at a single institution. *Pediatr Hematol Oncol* 1999; 16: 377-385.
- [23] A multicentre retrospective survey of Langerhans' cell histiocytosis: 348 cases observed between 1983 and 1993. The French Langerhans' Cell histiocytosis study group. *Arch Dis Child* 1996; 75: 17-24.
- [24] Moron FE, Morriss MC, Jones JJ and Hunter JV. Lumps and bumps on the head in children: use of CT and MR imaging in solving the clinical diagnostic dilemma. *Radiographics* 2004; 24: 1655-1674.
- [25] Tsuruda JS, Chew WM, Moseley ME and Norman D. Diffusion-weighted MR imaging of the brain: value of differentiating between extraaxial cysts and epidermoid tumors. *AJNR Am J Neuroradiol* 1990; 11: 925-931; discussion 932-924.
- [26] Annet L, Duprez T, Grandin C, Doods G, Collard A and Cosnard G. Apparent diffusion coefficient measurements within intracranial epidermoid cysts in six patients. *Neuroradiology* 2002; 44: 326-328.
- [27] Bastug D, Ortiz O and Schochet SS. Hemangiomas in the calvaria: Imaging findings. *AJR Am J Roentgenol* 1995; 164: 683-687.